# Constellation design of DFT-S-OFDM with dual-mode index modulation in VLC

CHEN CHEN,<sup>1,\*</sup> YUNGUI NIE,<sup>1</sup> FAHEEM AHMED,<sup>1</sup> ZHIHONG ZENG,<sup>2</sup> AND MIN LIU<sup>1</sup>

**Abstract:** In this paper, we for the first time propose a novel partitioning-based constellation design approach for discrete Fourier transform-spread-orthogonal frequency division multiplexing modulation with dual-mode index modulation (DFT-S-OFDM-DM) in visible light communication (VLC) systems. Specifically, two partitioning-based constellation designs, i.e., block-based constellation partitioning and interleaving-based constellation partitioning, are proposed to generate two distinguishable constellation sets for DFT-S-OFDM-DM in VLC, by considering four 8-ary constellations including 8-ary quadrature amplitude modulation (8-QAM), 8-ary phase-shift keying (8-PSK), circular (4,4)-QAM, and circular (7,1)-QAM. The superiority of DFT-S-OFDM-DM using circular (7,1)-QAM constellation with interleaving-based constellation partitioning over other benchmark schemes has been successfully verified by both simulation and experimental results. It is shown by the experimental results that a significant distance extension of 44.6% is obtained by DFT-S-OFDM-DM using circular (7,1)-QAM constellation with interleaving-based constellation partitioning in comparison to DFT-S-OFDM with index modulation achieving the same spectral efficiency of 2.5 bits/s/Hz. It is also demonstrated that the proposed constellation design schemes are also generally applicable to the constellation with an arbitrary shape and an arbitrary size.

© 2022 Optica Publishing Group under the terms of the Optica Open Access Publishing Agreement

## 1. Introduction

As one of the potential key enabling technologies for the sixth generation (6G) mobile networks and the Internet of Things (IoT) systems, visible light communication (VLC) has been triggering tremendous interest from both academia and industry in recent years [1,2]. Although VLC has many advantages such as abundant and unregulated spectrum resources, low-cost front-ends, electromagnetic interference-free operation and high physical-layer security [3], the development of high-speed VLC systems using commercially available LEDs is very challenging due to the limited modulation bandwidth and the severe nonlinearity of LEDs [4,5].

In order to improve the achievable data rate of practical VLC systems using commercial LEDs, many techniques have been reported in the literature. On the one hand, the bandwidth limitation of commercial LEDs can be addressed by the following two methods: one is to extend the LED modulation bandwidth through analog/digital and pre-/post-equalization [6,7], and the other is to increase the overall spectral efficiency for a given signal bandwidth via applying spectral-efficient modulation, multiplexing or multiple access techniques such as orthogonal frequency division multiplexing (OFDM) using high-order constellations [8,9], multiple-input multiple-output transmission [10,11], and non-orthogonal multiple access [12,13]. On the other hand, the LED nonlinearity issue can also be handled by the following two ways: one is to mitigate the nonlinear distortion by pre-/post-distortion [14,15], and the other is to transmit signals with low peak-to-average power ratio (PAPR) [16]. More specifically, discrete Fourier

#451780 Journal © 2022 https://doi.org/10.1364/OE.451780

<sup>&</sup>lt;sup>1</sup> School of Microelectronics and Communication Engineering, Chongqing University, Chongqing 400044, China

<sup>&</sup>lt;sup>2</sup>LiFi Research and Development Centre, Institute for Digital Communications, The University of Edinburgh, EH9 3JL, UK

<sup>\*</sup>c.chen@cqu.edu.cn

transform-spread OFDM (DFT-S-OFDM) has been widely shown as a promising technique for practical VLC systems, due to its advantages of high spectral efficiency and low PAPR [17–19].

Recently, OFDM with index modulation (OFDM-IM) has been introduced for VLC systems, which exhibits improved bit error rate (BER) performance than classical OFDM [20,21]. To increase the spectral efficiency and enhance the tolerance against LED nonlinearity, we have proposed a DFT-S-OFDM with quadrature index modulation scheme for practical VLC systems in our previous work [19]. Nevertheless, for OFDM with both index modulation and quadrature index modulation, there are a subset of subcarriers left unmodulated and the existence of these nulled subcarriers inevitably reduces the achievable spectral efficiency of the VLC system. Hence, to fully exploit the achievable spectral efficiency, OFDM with dual-mode index modulation (OFDM-DM) has been further applied in VLC systems, where all subcarriers are used to transmit constellation symbols [22]. The BER performance of OFDM-DM is highly affected by the adopted two distinguishable constellation sets and therefore constellation design plays a vital role in VLC systems using OFDM-DM. So far, several constellation design schemes have already been reported for OFDM-based VLC systems in the literature. In [23], a collaborated constellation design scheme has been proposed to improve the performance of OFDM-based VLC systems over the low-pass frequency-selective fading channel. In [24], an optimized constellation design scheme has been proposed for colour shift keying (CSK)-aided optical OFDM systems, which can not only improve the achievable BER performance but also eliminate the colour balance distortion issue. In [25], a superposed 32-ary quadrature amplitude modulation (32-QAM) constellation design has been proposed for OFDM-based spatial multiplexing VLC systems, so as to mitigate the adverse effect of high channel correlation. However, to the best of our knowledge, the constellation design issue in OFDM-DM-based VLC systems has been barely investigated in the literature.

In this paper, we propose and investigate a novel DFT-S-OFDM-DM scheme with partitioning-based constellation design for VLC systems. By taking the 8-ary constellation as an example, the proposed partitioning-based constellation design can be performed in the following two manners: one is block-based constellation partitioning and the other is interleaving-based constellation partitioning. Numerical simulations and hardware experiments have been conducted to evaluate the performance of VLC systems using DFT-S-OFDM-DM with partitioning-based constellation design and further compare with that using other benchmark schemes.

## 2. Principle of DFT-S-OFDM-IM and DFT-S-OFDM-DM

## 2.1. DFT-S-OFDM-IM

Figures 1(a) and 1(b) illustrate the block diagrams of DFT-S-OFDM-IM transmitter and receiver, respectively. As we can see, the m input bits are first partitioned into G groups via a bit splitter and each group has b bits, i.e., m = bG. Each group of b bits are further split into two parts, i.e.,  $b = b_1 + b_c$ , which are fed into an index selector and a constellation mapper to generate an OFDM subblock with length N, where  $N = N_{\text{data}}/G$  and  $N_{\text{data}}$  denotes the number of data subcarriers. More specifically, the first part of  $b_i$  bits are sent into the index selector to obtain the subcarrier index set  $I^{(\beta)}$  with length k for constellation mapping in the  $\beta$ -th subblock, where  $\beta = 1, \ldots, G$ . The second part of  $b_c$  bits are passed through the constellation mapper, which has the constellation set  $\mathcal{M} = [S_1, S_2, \ldots, S_M]$  with size M. The mapping table of DFT-S-OFDM-DM with N = 4 and k = 2 is given in Table 1. Hence, totally G subblocks are generated which are further concatenated by a subblock combiner to create a complete OFDM block. Subsequently, DFT spreading is performed to simultaneously reduce the PAPR of the signal and mitigate the low-pass effect of the VLC system. Finally, the transmitted DFT-S-OFDM-IM signal is obtained via inverse fast Fourier transform (IFFT) with the Hermitian symmetry (HS) constraint and parallel-to-serial (P/S) conversion.

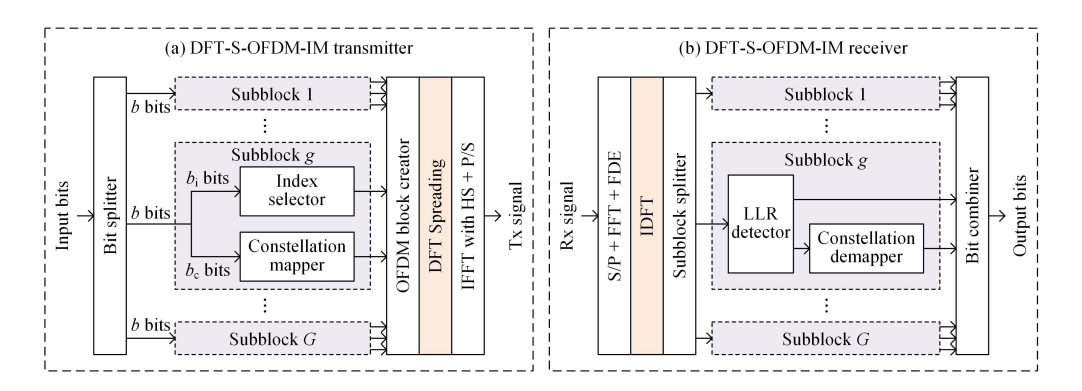


Fig. 1. Block diagrams of DFT-S-OFDM-IM (a) transmitter and (b) receiver.

Table 1. Mapping table of DFT-S-OFDM-IM for N=4 and k=2

Index bits	Index set for $\mathcal{M}$	Subblocks	
0 0	[1, 2]	$[S_i, S_j, 0, 0]$	
0 1	[2, 3]	$[0, S_i, S_j, 0]$	
1 1	[3, 4]	$[0,0,S_i,S_j]$	
10	[1, 4]	$[S_i, 0, 0, S_j]$	

In the DFT-S-OFDM-IM receiver, as shown in Fig. 1(b), the received DFT-S-OFDM-IM signal undergoes serial-to-parallel (S/P), FFT and frequency-domain equalization (FDE). After executing inverse DFT (IDFT), the OFDM block is split into G subblocks through a subblock splitter. In each subblock, a low-complexity log-likelihood ratio (LLR) detector is employed for signal detection [20]. Letting  $y^{\eta}_{\beta}$  ( $\beta=1,\ldots,G; \eta=1,\ldots,N$ ) denote the input signal, the corresponding LLR value for  $\beta$ -th subblock of the DFT-S-OFDM-IM signal is calculated by

$$\lambda_{\text{IM},\beta}^{\eta} = \ln(k) - \ln(N - k) + \ln\left(\sum_{i=1}^{M} \exp\left(-\frac{1}{N_0} \left| y_{\beta}^{\eta} - S_i \right|^2\right)\right). \tag{1}$$

According to the descriptions above, the number of index bits that can be transmitted per subblock is given by

$$b_{i} = \lfloor \log_{2}(C(N, k)) \rfloor, \qquad (2)$$

where  $\lfloor \cdot \rfloor$  represents the floor operator and  $C(\cdot, \cdot)$  denotes binomial coefficient. Moreover, the number of constellation bits carried by the constellation set  $\mathcal{M}$  is obtained by

$$b_{c} = k \log_{2}(M). \tag{3}$$

Hence, the spectral efficiency per OFDM block using DFT-S-OFDM-IM with *M*-QAM constellation is given by

$$SE_{\rm IM} = \frac{\left[\log_2(C(N,k))\right] + k\log_2(M)}{N}.$$
 (4)

#### 2.2. DFT-S-OFDM-DM

The block diagrams of DFT-S-OFDM-DM transmitter and receiver are illustrated in Figs. 2(a) and 2(b), respectively. In the DFT-S-OFDM-DM transmitter, the  $b_i$  bits are sent into the index

selector to divide the subcarrier indices of the  $\beta$ -th subblock into two index sets denoted as  $I_A^{(\beta)}$  and  $I_B^{(\beta)}$ , while the  $b_c$  bits are fed into two distinguishable constellation mappers A and B. The constellation mappers A and B have the constellation sets  $\mathcal{M}_A = [S_1^A, S_2^A, \dots, S_{M_A}^A]$  and  $\mathcal{M}_B = [S_1^B, S_2^B, \dots, S_{M_B}^B]$ , respectively. The sizes of  $\mathcal{M}_A$  and  $\mathcal{M}_B$  are respectively denoted by  $\mathcal{M}_A$  and  $\mathcal{M}_B$ , and we have  $\mathcal{M}_A \cap \mathcal{M}_B = \emptyset$ . The design of two distinguishable constellation sets  $\mathcal{M}_A$  and  $\mathcal{M}_B$  plays a vital role in DFT-S-OFDM-DM, which will be discussed in detail in Section 3.

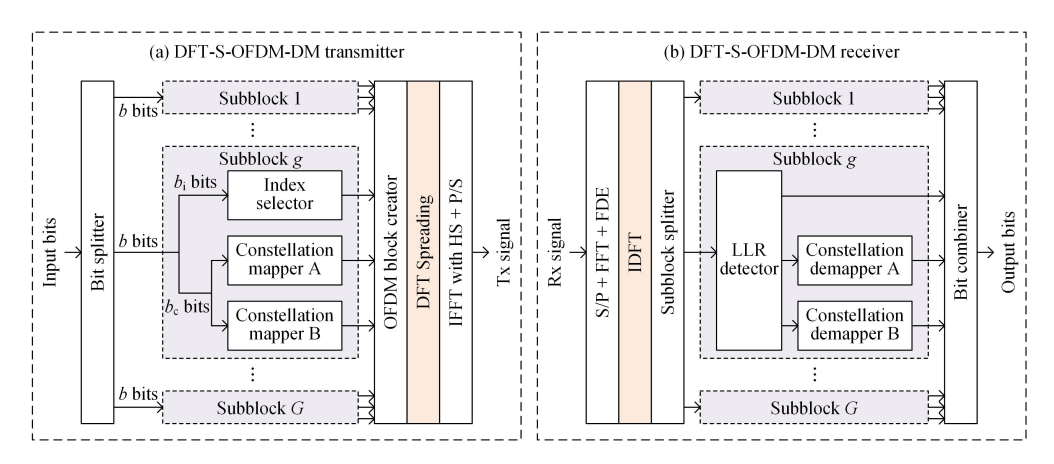


Fig. 2. Block diagrams of DFT-S-OFDM-DM (a) transmitter and (b) receiver.

With the aid of the index selector, the selected k subcarriers and the non-selected N-k subcarriers corresponding to  $I_A^{(\beta)}$  and  $I_B^{(\beta)}$  are modulated by the constellation mappers A and B, respectively. The mapping table of DFT-S-OFDM-DM with N=4 and k=2 is given in Table 2. Moreover, letting  $y_\beta^\eta$  ( $\beta=1,\ldots,G;\eta=1,\ldots,N$ ) denote the input signal, the corresponding LLR value for  $\beta$ -th subblock of the DFT-S-OFDM-DM signal is given by [22]

$$\lambda_{\text{DM},\beta}^{\eta} = \ln(k) - \ln(N - k) + \ln\left(\sum_{i=1}^{M_{A}} \exp\left(-\frac{1}{N_{0}} \left| y_{\beta}^{\eta} - S_{i}^{A} \right|^{2}\right)\right) - \ln\left(\sum_{j=1}^{M_{B}} \exp\left(-\frac{1}{N_{0}} \left| y_{\beta}^{\eta} - S_{j}^{B} \right|^{2}\right)\right), (5)$$

Table 2. Mapping table of DFT-S-OFDM-DM for N=4 and k=2

Index bits	Index set for $\mathcal{M}_A$	Index set for $\mathcal{M}_{\mathrm{B}}$	Subblocks
0.0	[1, 2]	[3, 4]	$[S_i^{\text{A}}, S_j^{\text{A}}, S_i^{\text{B}}, S_j^{\text{B}}]$
0 1	[2, 3]	[1, 4]	$[S_i^{\mathrm{B}}, S_i^{\mathrm{A}}, S_j^{\mathrm{A}}, S_j^{\mathrm{B}}]$
1 1	[3, 4]	[1, 2]	$[S_i^{\mathrm{B}}, S_j^{\mathrm{B}}, S_i^{\mathrm{A}}, S_j^{\mathrm{A}}]$
10	[1, 4]	[2, 3]	$[S_i^{\text{A}}, S_i^{\text{B}}, S_j^{\text{B}}, S_j^{\text{A}}]$

For DFT-S-OFDM-DM, the constellation bits are carried by the two distinguishable constellation sets  $\mathcal{M}_A$  and  $\mathcal{M}_B$  and hence the spectral efficiency of each OFDM block using DFT-S-OFDM-DM with constellation sets  $\mathcal{M}_A$  and  $\mathcal{M}_B$  is expressed by

$$SE_{\rm DM} = \frac{\left \lfloor \log_2(C(N,k)) \right \rfloor + k \log_2(M_{\rm A}) + (N-k) \log_2(M_{\rm B})}{N}. \tag{6}$$

## 3. Partitioning-based constellation design for DFT-S-OFDM-DM

The performance of VLC systems applying DFT-S-OFDM-DM is largely determined by the adopted two distinguishable constellation sets  $\mathcal{M}_A$  and  $\mathcal{M}_B$ . In this section, we propose a novel partitioning-based constellation design for DFT-S-OFDM-DM in VLC systems.

To introduce the proposed partitioning-based constellation design, we first consider four 8-ary constellations including conventional 8-ary QAM (8-QAM) and 8-ary phase-shift keying (8-PSK), and special-shaped circular (4,4)-QAM [26] and circular (7,1)-QAM [27]. Figures 3(a)–3(d) show the constellation diagram of 8-QAM, 8-PSK, circular (4,4)-QAM and circular (7,1)-QAM, respectively. Utilizing these 8-ary constellations, two distinguishable 4-ary constellation sets  $\mathcal{M}_A$  and  $\mathcal{M}_B$  with  $\mathcal{M}_A = \mathcal{M}_B = 4$  can be obtained via constellation partitioning.

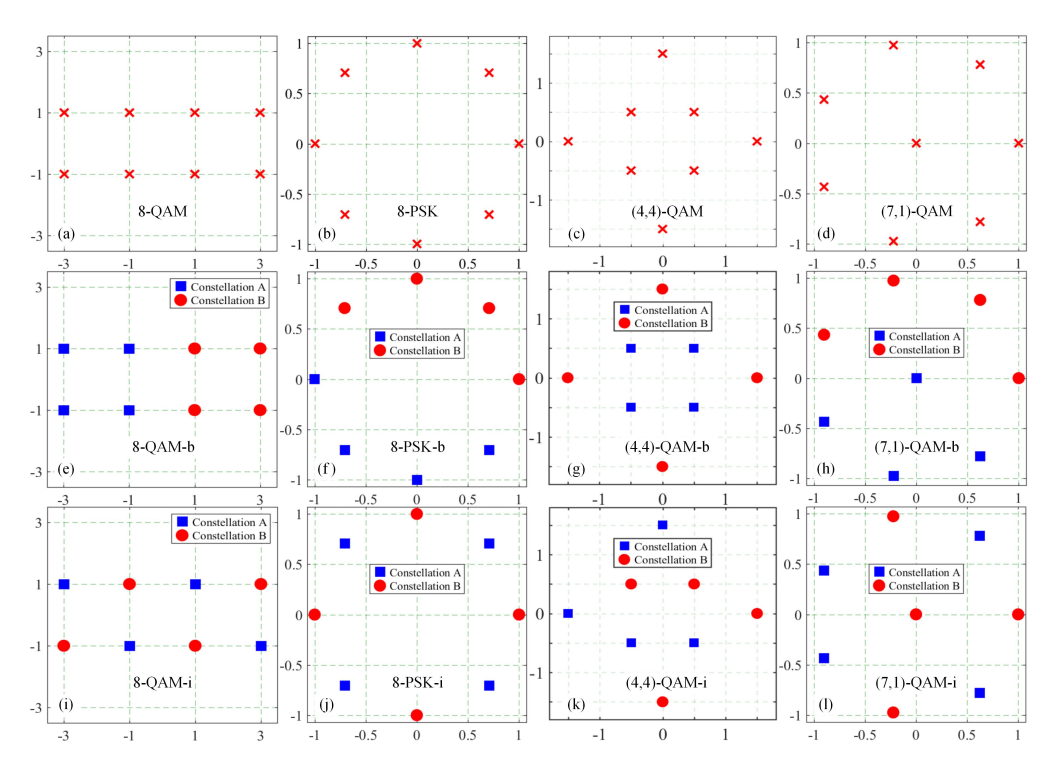


**Fig. 3.** Constellation diagrams of (a) 8-QAM, (b) 8-PSK, (c) circular (4,4)-QAM, (d) circular (7,1)-QAM, block-based constellation partitioning for (e) 8-QAM-b, (f) 8-PSK-b, (g) circular (4,4)-QAM-b, (h) circular (7,1)-QAM-b, and interleaving-based constellation partitioning for (i) 8-QAM-i, (j) 8-PSK-i, (k) circular (4,4)-QAM-i, (l) circular (7,1)-QAM-i.

Specifically, constellation partitioning can be performed in the following two manners: one is block-based partitioning and the other is interleaving-based partitioning. For block-based constellation partitioning, the 8-ary constellation is divided into two 4-ary sub-constellations in a block-by-block manner. For simplicity of notation, we define 8-QAM, 8-PSK, circular (4,4)-QAM and circular (7,1)-QAM with block-based partitioning as 8-QAM-b, 8-PSK-b, circular (4,4)-QAM-b and circular (7,1)-QAM-b, respectively. For interleaving-based constellation partitioning, the 8-ary constellation is partitioned into two 4-ary sub-constellations in an interleaved manner. For simplicity of notation, 8-QAM, 8-PSK, circular (4,4)-QAM and circular (7,1)-QAM with interleaving-based partitioning are defined as 8-QAM-i, 8-PSK-i, circular (4,4)-QAM-i and (7,1)-QAM-i, respectively. Figures 3(e)-3(l) show the corresponding constellation diagrams of 8-QAM-b, 8-PSK-b, circular (4,4)-QAM-b, circular (7,1)-QAM-b, 8-QAM-i, 8-PSK-i, circular

(4,4)-QAM-i and circular (7,1)-QAM-i, respectively. It can be clearly observed from Fig. 3 that the minimum Euclidean distance of each 4-ary sub-constellation obtained by interleaving-based partitioning is relatively larger than that obtained by block-based partitioning for all four 8-ary constellations including 8-QAM, 8-PSK, circular (4,4)-QAM and circular (7,1)-QAM. Moreover, it also demonstrates that the proposed constellation design schemes can be applied to the constellation with an arbitrary shape.

Although only 8-ary constellations are discussed above, the proposed constellation design schemes are generally applicable to the constellation with an arbitrary size. To demonstrate its general applicability, we further consider the following constellations to perform the proposed partitioning-based constellation design, i.e., 4-QAM, 16-QAM, 32-QAM and 64-QAM. Figures 4(a)–4(l) show the corresponding constellation diagrams of 4-QAM, 16-QAM, 32-QAM and 64-QAM with block-based partitioning and interleaving-based partitioning, respectively. Similarly, for each constellation, a relatively larger minimum Euclidean distance can be obtained by the sub-constellation when applying interleaving-based partitioning.

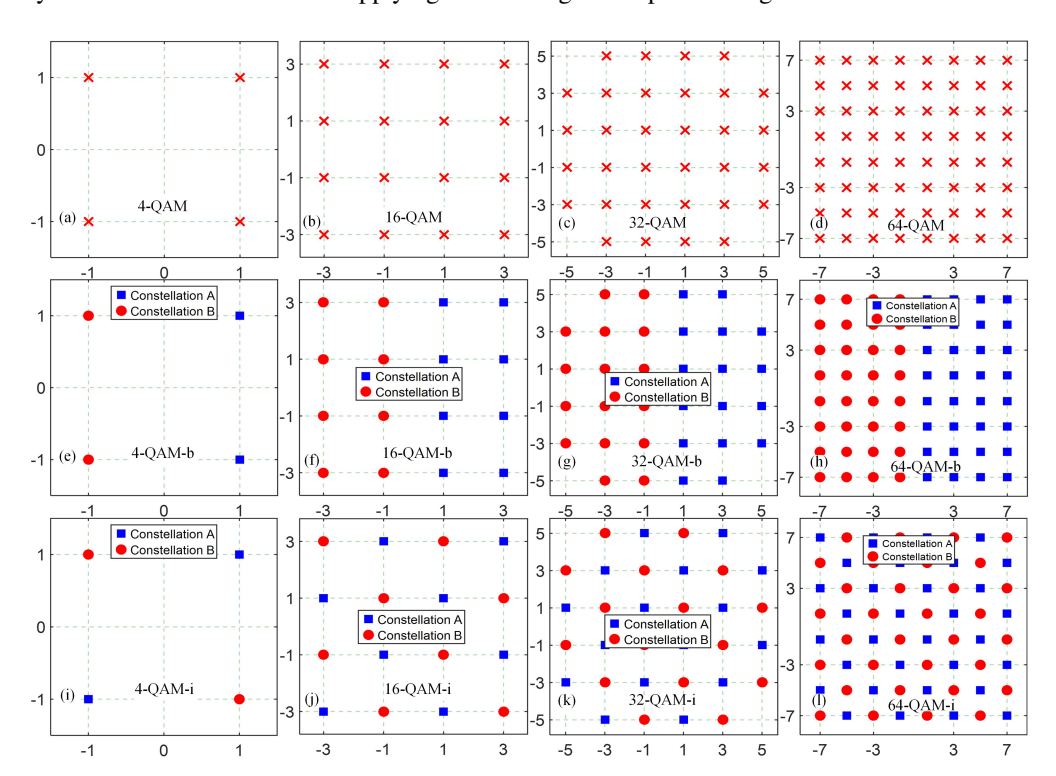


**Fig. 4.** Constellation diagrams of (a) 4-QAM, (b) 16-QAM, (c) 32-QAM, (d) 64-QAM, block-based constellation partitioning for (e) 4-QAM-b, (f) 16-QAM-b, (g) 32-QAM-b, (h) 64-QAM-b, and interleaving-based constellation partitioning for (i) 4-QAM-i, (j) 16-QAM-i, (k) 32-QAM-i, (l) 64-QAM-i.

As the proposed constellation design schemes are directly applicable to the constellation with an arbitrary shape and an arbitrary size, and constellation optimization is not required. Therefore, the proposed constellation design schemes are simple and efficient, which are promising for practical high-speed and low-complexity VLC systems applying DFT-S-OFDM-DM.

## 4. Results and discussions

In this section, we evaluate and compare the performance of VLC systems applying DFT-S-OFDM-DM with the following constellation designs including 8-QAM-b, 8-QAM-i, 8-PSK-b, 8-PSK-i, circular (4,4)-QAM-b, circular (4,4)-QAM-i, circular (7,1)-QAM-b and circular (7,1)-QAM-i through both numerical simulations and hardware experiments. For the purpose of comparison, conventional OFDM and OFDM-IM are also considered in the performance evaluation. In both simulations and experiments, the length of IFFT/FFT and the number of data subcarriers are set to 256 and 92, respectively. Moreover, the size of each OFDM subblock is N=4 and the number of selected subcarriers to transmit  $\mathcal{M}_A$  is k=2.

#### 4.1. Simulation results

In our simulations, we first investigate the BER performance of OFDM-DM with the abovementioned 8-ary constellation designs achieving a spectral efficiency of 2.5 bits/s/Hz and compare it with conventional OFDM and OFDM-IM over the additive white Gaussian noise (AWGN) channel. According to (4), the spectral efficiency of DFT-S-OFDM-DM with  $M_A = M_B = 4$ , N = 4 and k = 2 is 2.5 bits/s/Hz. To achieve the same spectral efficiency of 2.5 bits/s/Hz, as per (5), 16-QAM constellation needs to be used in DFT-S-OFDM-IM. Nevertheless, it is impossible for conventional OFDM to achieve a spectral efficiency of 2.5 bits/s/Hz. It should be noted that the BER performance of these modulation schemes remains the same over the AWGN channel without and with DFT spreading. Figure 5 shows the simulation BER versus signal-to-noise ratio (SNR) for OFDM, OFDM-IM and OFDM-DM with different 8-ary constellation designs over the AWGN channel. For conventional OFDM, 4-QAM and 8-QAM constellations are considered which are corresponding to spectral efficiencies of 2 and 3 bits/s/Hz, respectively. As we can see, OFDM with 4-QAM performs the best while OFDM with 8-QAM performs the worst among all the schemes. It can be further observed that OFDM-DM greatly outperforms OFDM-IM with 16-QAM when a proper constellation design is employed. Particularly, for a given 8-ary constellation, OFDM-DM with interleaving-based constellation design always outperforms that with block-based constellation design. Moreover, circular (7,1)-QAM is shown to be the best choice for OFDM-DM among all the four 8-ary constellations. To reach the 7% forward error correction (FEC) coding limit of BER =  $3.8 \times 10^{-3}$ , the required SNRs for 8-QAM-b, 8-QAM-i, 8-PSK-b, 8-PSK-i, circular (4,4)-QAM-b, circular (4,4)-QAM-i, circular (7,1)-QAM-b and circular (7,1)-QAM-i are 11.6, 10.8, 11.8, 11.1, 11.0, 10.4, 10.2 and 9.8 dB, respectively. As a result, SNR gains of 1.0 and 1.3 dB can be achieved by circular (7,1)-QAM-i in comparison to 8-QAM-i and 8-PSK-i, respectively. Moreover, circular (7,1)-QAM-i also outperforms circular (7,1)-QAM-b by an SNR gain of 0.4 dB. Therefore, OFDM-DM with circular (7,1)-QAM-i achieves the best BER performance among all the OFDM-DM schemes with a spectral efficiency of 2.5 bits/s/Hz.

We further compare the PAPR performance of OFDM, OFDM-IM and OFDM-DM without and with DFT spreading, and Fig. 6 shows the complementary cumulative distribution function (CCDF) versus PAPR for different schemes without and with DFT spreading. It can be seen that the use of DFT spreading can significantly reduce the PAPR of all the schemes. Specifically, at a probability of 10<sup>-3</sup>, PAPR reductions of 3.2 and 1.7 dB are achieved by OFDM with 4-QAM and 8-QAM after performing DFT spreading, respectively. However, the PAPR reduction at a probability of 10<sup>-3</sup> is only about 1 dB for OFDM-IM with 16-QAM. For OFDM-DM, substantial PAPR reductions of 3.6, 1.7, 4.5, 3.4, 2.5, 2.2, 4.2 and 3.0 dB at a probability of 10<sup>-3</sup> are respectively obtained by 8-QAM-b, 8-QAM-i, 8-PSK-b, 8-PSK-i, circular (4,4)-QAM-b, circular (4,4)-QAM-i, circular (7,1)-QAM-b and circular (7,1)-QAM-i constellations when DFT spreading is executed. Therefore, DFT spreading is an efficient way to significantly reduce the PAPR of OFDM-DM signals, and VLC systems applying DFT-S-OFDM-DM with a proper constellation design can exhibit enhanced tolerance against LED nonlinearity.

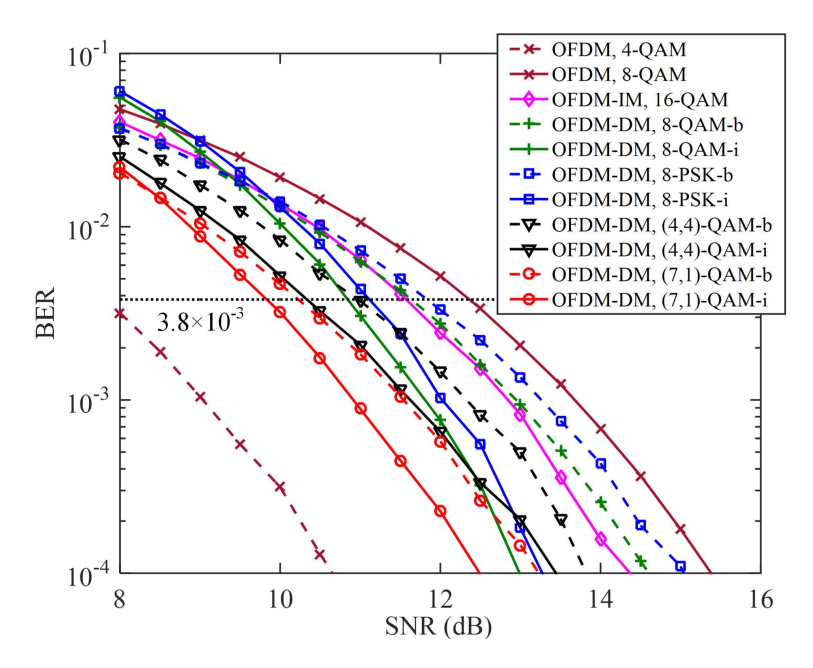


**Fig. 5.** Simulation BER vs. SNR for OFDM, OFDM-IM and OFDM-DM with different 8-ary constellation designs over the AWGN channel.

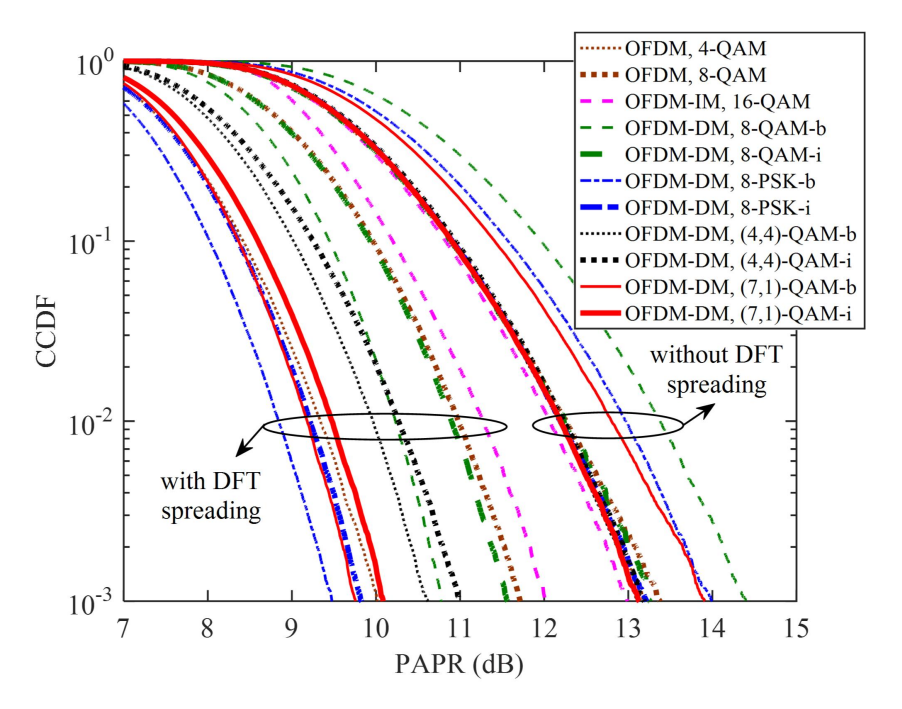


**Fig. 6.** PAPR comparison of OFDM, OFDM-IM and OFDM-DM without and with DFT spreading.

Figures 7(a)–7(d) show the simulation BER versus SNR for OFDM-IM and OFDM-DM for the spectral efficiencies of 1.5, 3.5, 4.5 and 5.5 bits/s/Hz, respectively, over the AWGN channel. For the spectral efficiency of 1.5 bits/s/Hz, OFDM-DM with 4-QAM-i achieves the same BER performance as OFDM-IM with 4-QAM. Moreover, it can be clearly seen that OFDM-DM greatly outperforms OFDM-IM to achieve the same target spectral efficiency. More specifically, OFDM-DM with 4-QAM-i, 16-QAM-i, 32-QAM-i and 64-QAM-i outperforms OFDM-DM with 4-QAM-b, 16-QAM-b, 32-QAM-b and 64-QAM-b at BER =  $3.8 \times 10^{-3}$  by SNR gains of 0.89, 0.85, 0.73 and 0.50 dB, respectively. It indicates that the SNR gain is gradually reduced with the increase of the spectral efficiency.

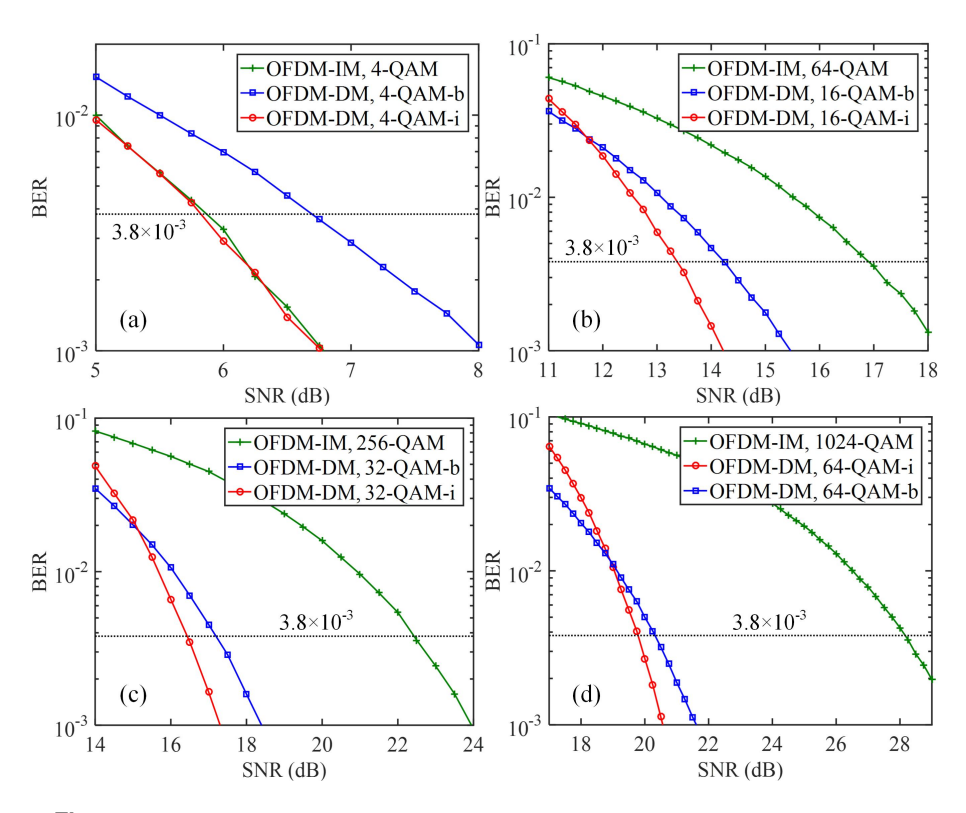


**Fig. 7.** Simulation BER vs. SNR for OFDM-IM and OFDM-DM for the spectral efficiencies of (a) 1.5, (b) 3.5, (c) 4.5, and (d) 5.5 bits/s/Hz over the AWGN channel.

## 4.2. Experimental results

In this subsection, we experimentally investigate the performance of DFT-S-OFDM-DM with two 8-ary interleaving-based constellation designs, i.e., 8-PSK-i and circular (7,1)-QAM-i, in a practical bandlimited nonlinear VLC system. For performance comparison, the following four schemes are considered as benchmark schemes: 1) OFDM-IM with 16-QAM, 2) DFT-S-OFDM-IM with 16-QAM, 3) OFDM-DM with 8-PSK-i and 4) OFDM-DM with circular (7,1)-QAM-i. Figure 8 depicts the experimental setup and the photo of a point-to-point VLC system using a blue mini-LED. As can be seen, the transmitted signal, which is generated offline by MATLAB, is first sent to an arbitrary waveform generator (AWG, Tektronix AFG31102) with a sampling rate of 250 MSa/s. Then, a DC bias current of 120 mA is combined with the AWG output signal via a bias-tee (bias-T, Mini-Circuits ZFBT-6GW+) to drive a blue mini-LED (HCCLS2021CHI03). The light emitted by the LED passes through a biconvex lens and propagates over the free-space

channel. At the receiver side, another biconvex lens is used to focus the light onto the active area of a photodetector (PD, Thorlabs PDA10A2). Subsequently, the output electrical signal of the PD is recorded by a digital storage oscilloscope (DSO, LeCroy WaveSurfer 432) with a sampling rate of 1 GSa/s and the resultant digital signal is further processed offline in MATLAB. In OFDM modulation, the length of IFFT/FFT is 256 and the number of data subcarriers is 92. Hence, the bandwidth of the AWG output signal is about 90 MHz and the data rate of the VLC system using DFT-S-OFDM-DM with 8-PSK-i and circular (7,1)-QAM-i is about 225 Mbits/s.

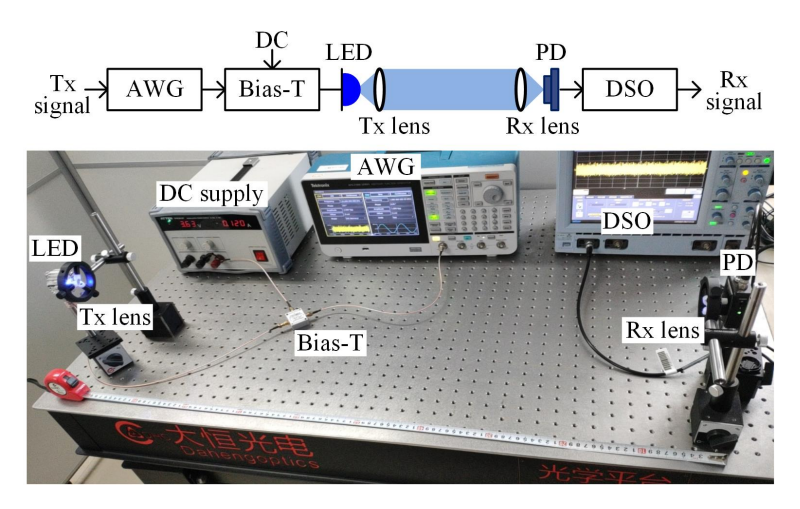
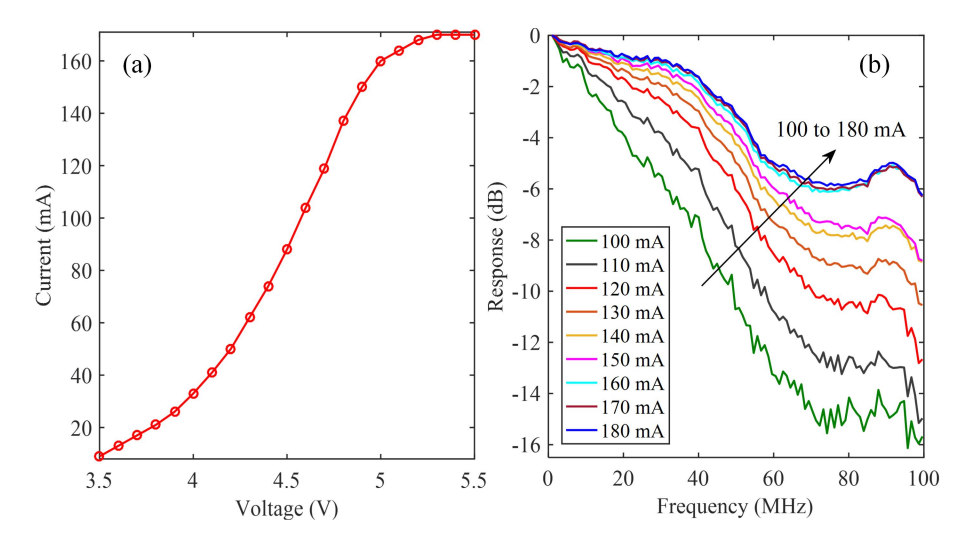


Fig. 8. Experimental setup of a point-to-point VLC system using a blue mini-LED.

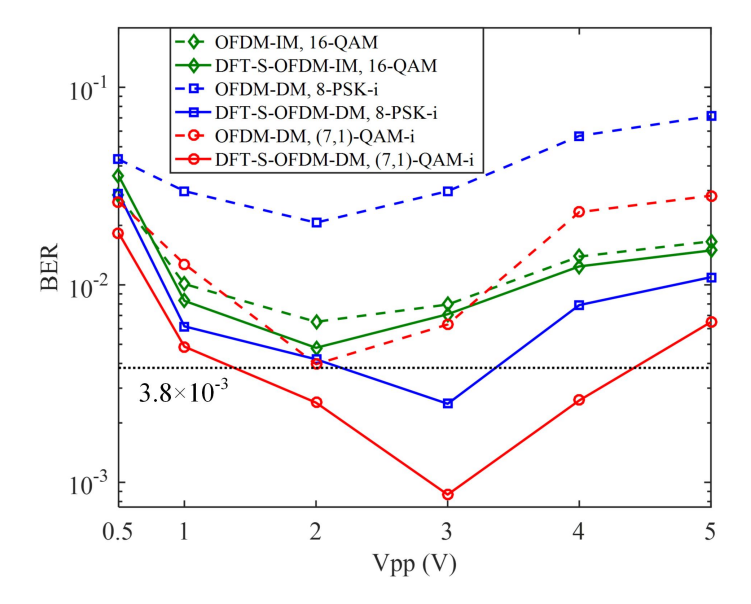
The measured nonlinear current-voltage curve and the frequency response with different bias currents ranging from 100 to 180 mA with a step of 10 mA are given in Figs. 9(a) and 9(b), respectively. It can be clearly seen from Fig. 9(a) that the experimental system suffers from notable nonlinearity which is mainly due to the use of the blue mini-LED. Moreover, the current becomes stable at about 170 mA when the voltage reaches 5.3 V and further increasing the voltage cannot lead to the increase of the current. Hence, the peaks of the modulation signal might be clipped if the applied peak-to-peak voltage (Vpp) is too large. Furthermore, as shown in Fig. 9(b), the experimental system exhibits a typically low-pass frequency response and a larger bandwidth can be obtained with a higher bias current. As a trade-off between bandwidth and feasible dynamic range, the bias current is set to 120 mA and the corresponding –3dB bandwidth is about 35 MHz.

Figure 10 shows the measured BER versus the Vpp for different schemes with a transmission distance of 80 cm. As we can see, the BER of DFT-S-OFDM-IM is slightly better than that of OFDM-IM. Moreover, DFT-S-OFDM-DM with both 8-PSK-i and circular (7,1)-QAM-i greatly outperforms OFDM-IM and DFT-S-OFDM-IM when Vpp is relatively large. Particularly, OFDM-IM, DFT-S-OFDM-IM, and OFDM-DM with both 8-PSK-i and circular (7,1)-QAM-i obtain their lowest BERs at the same Vpp of 2 V, while DFT-S-OFDM-DM with both 8-PSK-i and circular (7,1)-QAM-i achieves the lowest BERs at the same Vpp of 3 V. Hence, the optimal Vpp for DFT-S-OFDM-DM with both 8-PSK-i and circular (7,1)-QAM-i is larger than that of other benchmark schemes, indicating its enhanced robustness against LED nonlinearity. In addition, the corresponding constellation diagrams of different schemes are given in Fig. 11.

Finally, we investigate the BER versus transmission distance for different schemes and the measured results are shown in Fig. 12. It can be seen that the BERs of OFDM-IM and OFDM-DM with 8PSK-i cannot reach the FEC limit of  $3.8 \times 10^{-3}$  within the distance range from 60 to 100 cm. Moreover, the maximum distances that can be transmitted by DFT-S-OFDM-IM and



**Fig. 9.** Measured (a) nonlinear current-voltage curve and (b) frequency response with different bias currents.



 $\textbf{Fig. 10.} \ \ \text{Measured BER vs. Vpp for different schemes with a transmission distance of 80 cm.}$ 

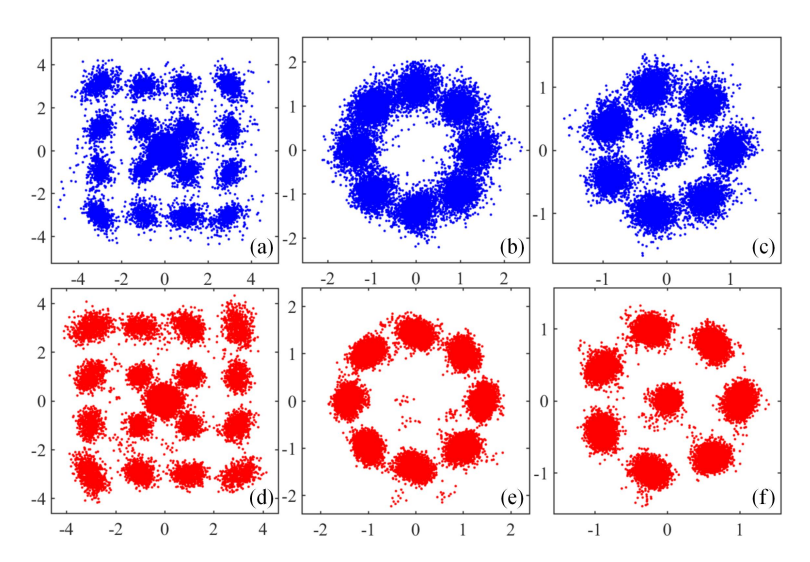


**Fig. 11.** Measured constellation diagrams of (a) OFDM-IM with 16-QAM and Vpp=2V, (b) OFDM-DM with 8-PSK-i and Vpp=2V, (c) OFDM-DM with (7,1)-QAM-i and Vpp=2V, (d) DFT-S-OFDM-IM with 16-QAM and Vpp=2V, (e) DFT-S-OFDM-DM with 8-PSK-i and Vpp=3V, and (f) DFT-S-OFDM-DM with (7,1)-QAM-i and Vpp=3V.

OFDM-DM with circular (7,1)-QAM-i, DFT-S-OFDM-DM with 8-PSK-i and DFT-S-OFDM-DM with circular (7,1)-QAM-i below BER =  $3.8 \times 10^{-3}$  are 67.5, 78.5, 90.6 and 97.6 cm, respectively. Hence, a significant distance extension of 44.6% is obtained by DFT-S-OFDM-DM with circular (7,1)-QAM-i in comparison to DFT-S-OFDM-IM. Moreover, the transmission distance is extended by 24.3% for OFDM-DM with circular (7,1)-QAM-i when DFT spreading is performed. For DFT-S-OFDM-DM, the use of circular (7,1)-QAM-i constellation design leads to a distance extension of 7.7% compared with the 8-PSK-i constellation design. Therefore, the

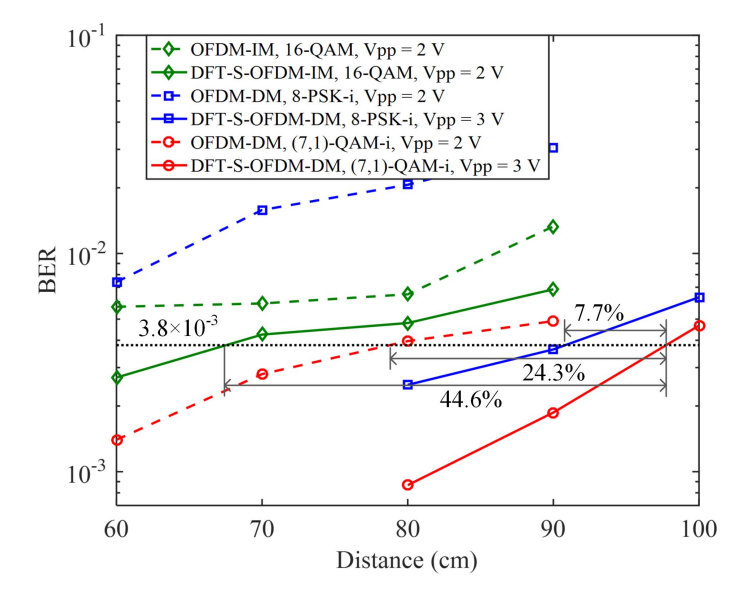


Fig. 12. Measured BER vs. transmission distance for different schemes.

performance of VLC systems employing OFDM-DM can be substantially improved by applying the circular (7,1)-QAM-i constellation design with DFT spreading.

#### 5. Conclusion

In this paper, we have proposed and evaluated a novel DFT-S-OFDM-DM scheme with partitioning-based constellation design for VLC systems. By employing three 8-ary constellations including 8-QAM, 8-PSK and circular (7,1)-QAM, two partitioning-based constellation designs, i.e., block-based constellation partitioning and interleaving-based constellation partitioning, are proposed to generate two distinguishable 4-ary constellation sets for DFT-S-OFDM-DM in VLC. Both simulation and experimental results verify the superiority of DFT-S-OFDM-DM using circular (7,1)-QAM constellation with interleaving-based constellation partitioning in comparison to other benchmark schemes. Moreover, it is also shown that the proposed constellation design schemes are generally applicable to the constellation with an arbitrary shape and an arbitrary size. Therefore, DFT-S-OFDM-DM using interleaving-based constellation partitioning can be a promising candidate for practical high-speed and low-complexity VLC systems.

**Funding.** National Natural Science Foundation of China (61901065); Fundamental Research Funds for the Central Universities (2021CDJQY-013); China Postdoctoral Science Foundation (2021M693744); Natural Science Foundation of Chongqing (cstc2021jcyj-msxmX0480).

**Disclosures.** The authors declare that there are no conflicts of interest related to this article.

**Data availability.** The data underlying the results presented in this paper are not publicly available at this time but may be obtained from the authors upon reasonable request.

#### References

- N. Chi, Y. Zhou, Y. Wei, and F. Hu, "Visible light communication in 6G: Advances, challenges, and prospects," IEEE Veh. Technol. Mag. 15(4), 93–102 (2020).
- I. Demirkol, D. Camps-Mur, J. Paradells, M. Combalia, W. Popoola, and H. Haas, "Powering the Internet of Things through light communication," IEEE Commun. Mag. 57(6), 107–113 (2019).
- T. Komine and M. Nakagawa, "Fundamental analysis for visible-light communication system using LED lights," IEEE Trans. Consum. Electron. 50(1), 100–107 (2004).
- 4. L. Grobe, A. Paraskevopoulos, J. Hilt, D. Schulz, F. Lassak, F. Hartlieb, C. Kottke, V. Jungnickel, and K.-D. Langer, "High-speed visible light communication systems," IEEE Commun. Mag. 51(12), 60–66 (2013).
- K. Ying, Z. Yu, R. J. Baxley, H. Qian, G.-K. Chang, and G. T. Zhou, "Nonlinear distortion mitigation in visible light communications," IEEE Wireless Commun. 22(2), 36–45 (2015).
- H. Le Minh, D. O'Brien, G. Faulkner, L. Zeng, K. Lee, D. Jung, Y. Oh, and E. T. Won, "100-Mb/s NRZ visible light communications using a postequalized white LED," IEEE Photonics Technol. Lett. 21(15), 1063–1065 (2009).
- C. Chen, Y. Nie, M. Liu, Y. Du, R. Liu, Z. Wei, H. Y. Fu, and B. Zhu, "Digital pre-equalization for OFDM-based VLC systems: Centralized or distributed?" IEEE Photonics Technol. Lett. 33(19), 1081–1084 (2021).
- 8. R. Mesleh, H. Elgala, and H. Haas, "On the performance of different OFDM based optical wireless communication systems," J. Opt. Commun. Netw. 3(8), 620–628 (2011).
- A. A. Purwita, M. D. Soltani, M. Safari, and H. Haas, "Terminal orientation in OFDM-based LiFi systems," IEEE Trans. Wireless Commun. 18(8), 4003

  –4016 (2019).
- T. Fath and H. Haas, "Performance comparison of MIMO techniques for optical wireless communications in indoor environments," IEEE Trans. Commun. 61(2), 733–742 (2013).
- C. Chen, X. Zhong, S. Fu, X. Jian, M. Liu, H. Yang, A. Alphones, and H. Y. Fu, "OFDM-based generalized optical MIMO," J. Lightwave Technol. 39(19), 6063–6075 (2021).
- H. Marshoud, V. M. Kapinas, G. K. Karagiannidis, and S. Muhaidat, "Non-orthogonal multiple access for visible light communications," IEEE Photonics Technol. Lett 28(1), 51–54 (2016).
- C. Chen, S. Fu, X. Jian, M. Liu, X. Deng, and Z. Ding, "NOMA for energy-efficient LiFi-enabled bidirectional IoT communication," IEEE Trans. Commun. 69(3), 1693–1706 (2021).
- X. Deng, S. Mardanikorani, Y. Wu, K. Arulandu, B. Chen, A. M. Khalid, and J.-P. M. G. Linnartz, "Mitigating LED nonlinearity to enhance visible light communications," IEEE Trans. Commun. 66(11), 5593–5607 (2018).
- C. Chen, X. Deng, Y. Yang, P. Du, H. Yang, and L. Zhao, "LED nonlinearity estimation and compensation in VLC systems using probabilistic Bayesian learning," Appl. Sci. 9(13), 2711 (2019).
- W. O. Popoola, Z. Ghassemlooy, and B. G. Stewart, "Pilot-assisted PAPR reduction technique for optical OFDM communication systems," J. Lightwave Technol. 32(7), 1374–1382 (2014).

- 17. M. Shi, C. Wang, H. Guo, Y. Wang, X. Li, and N. Chi, "A high-speed visible light communication system based on DFT-S OFDM," in *IEEE Int. Conf. Commun. Syst.*, (ICCS, 2016), pp. 1–5.
- 18. Z.-Y. Wu, Y.-L. Gao, Z.-K. Wang, C. You, C. Yang, C. Luo, and J. Wang, "Optimized DFT-spread OFDM based visible light communications with multiple lighting sources," Opt. Express 25(22), 26468–26482 (2017).
- F. Ahmed, Y. Nie, C. Chen, M. Liu, P. Du, and A. Alphones, "DFT-spread OFDM with quadrature index modulation for practical VLC systems," Opt. Express 29(21), 33027–33036 (2021).
- 20. E. Başar and E. Panayırcı, "Optical OFDM with index modulation for visible light communications," in *IEEE Int. Workshops Opt. Wireless Commun.*, (IWOW, 2015), pp. 11–15.
- C. Chen, X. Deng, Y. Yang, P. Du, H. Yang, and W.-D. Zhong, "Experimental demonstration of optical OFDM with subcarrier index modulation for IM/DD VLC," in *Asia Communications and Photonics Conference*, (ACP, 2019), p. M4A.40.
- T. Mao, R. Jiang, and R. Bai, "Optical dual-mode index modulation aided OFDM for visible light communications," Opt. Commun. 391, 37–41 (2017).
- 23. D.-F. Zhang, Y.-J. Zhu, J.-K. Zhang, and Y.-Y. Zhang, "Constellation collaborated OFDM for visible light communication systems," IEEE Commun. Lett. 18(6), 1067–1070 (2014).
- Z. Lin, M. Jiang, and H.-Z. Tan, "Constellation design for complex colour shift keying aided optical OFDM systems," in *IEEE 88th Vehicular Technology Conference*, (VTC-Fall, 2018), pp. 1–5.
- 25. X. Guo and N. Chi, "Superposed 32QAM constellation design for 2×2 spatial multiplexing MIMO VLC systems," J. Lightwave Technol. 38(7), 1702–1711 (2020).
- 26. X. Zhou, J. Yu, M.-F. Huang, Y. Shao, T. Wang, P. Magill, M. Cvijetic, L. Nelson, M. Birk, G. Zhang, S. Ten, H. B. Matthew, and S. K. Mishra, "32Tb/s (320×114Gb/s) PDM-RZ-8QAM transmission over 580km of SMF-28 ultra-low-loss fiber," in *Opt. Fiber Commun. Conf.*, (OFC, 2009), p. PDPB4.
- 27. J. Zhao, C. Qin, M. Zhang, and N. Chi, "Investigation on performance of special-shaped 8-quadrature amplitude modulation constellations applied in visible light communication," Photonics Res. 4(6), 249–256 (2016).